



# Rotating Permanent Magnets Based Flux Pump for HTS No-Insulation Coil

Jun Ma , Jianzhao Geng , Jamie Gawith, Heng Zhang, Chao Li , Boyang Shen , Qihuan Dong, Jiabin Yang, Jie Chen, Zhaokai Li , and Tim A. Coombs 

**Abstract**—High-temperature superconducting (HTS) no-insulation (NI) coil is a promising design because of high current density, high thermal stability, and self-protection mechanism. Flux pumping is a contactless charging method for a superconducting magnet, which can reduce the cryogenic losses associated with current leads. In this study, we compared the charging performance of a rotating permanent magnets-based flux pump for two different types of HTS coils: an INS coil and an NI coil. Results showed that the rotating type flux pump works well with both coils. But the charging speed of NI coil is much slower, which results from the small parallel characteristic resistance of NI coil. Results also show that the output DC voltage and inherent dynamic resistance of the flux pump increase linearly with the increase of rotating speed.

**Index Terms**—High temperature superconductor, no insulation coil, flux pump.

## I. INTRODUCTION

HIGH temperature superconducting (HTS) magnets have great potential in many applications: such as NMR/MRI [1], levitation system [2], [3], and high field applications [4], [5]. HTS magnets can be wound with two different techniques: winding HTS magnet with turn-to-turn insulation is a traditional technique to prevent short circuit in between turns. A new no insulation winding design is firstly proposed by Hahn [6]. This no insulation design has excellent electrical and thermal stability, self-protection ability, and compact size [6]–[10]. However, a significant slow charging speed is a major problem of the NI magnet, due to the current bypass through the characteristic resistance ( $R_c$ ) [6], [8], [9], [11].

Normally HTS magnets have to be consistently maintained by external power supplies, because of the joint loss and flux creep in superconductor. Flux pumping is an alternative charging method that can inject flux into closed superconducting circuit in a contactless manner. Flux pump can make HTS magnets working in a quasi-persistent current mode, which is of huge po-

tential for the large high field magnet. Several types of HTS flux pump have been proposed and developed: rotating permanent magnets based flux pump [12]–[16], linear travelling wave flux pump [17], [18], and AC field controlled transformer-rectifier flux pump [19], [20].

Rotating permanent magnets based flux pump was firstly proposed by Hoffman [12]. It has a very simple design and gained much popularity during these years. The rotating permanent magnets based flux pump functions as a DC voltage source with an inherent resistance ( $R_d$ ) [12], [13], [21]. Many impacting factors on the output performance have been investigated and analyzed, such as: frequency [22], [23], geometry of flux gap [23], stator wire [25], magnet [26], and annular yoke [27]. This type of flux pump has shown huge potential in many HTS applications, such as HTS wind generator [15], [28] and HTS motor [29], [30], HTS coil magnet [14] and stack tapes magnets [31].

Recently, a study on charging characteristics of a rotating permanent magnets based flux pump for NI magnet had already been presented [32]. A detailed and comprehensive comparison of charging process between NI and INS coil was presented. It demonstrated the feasibility of employing the rotating permanent magnets based flux pump to energize the NI coil magnet.

In our group, we have already presented a comprehensive analysis on the charging characteristic of HTS transformer-rectifier flux pump for the NI magnet [33] and further improvement was made [34]. In this work, we investigated the charging performance of a rotating permanent magnets based flux pump for the low  $R_c$  NI and INS coil magnets. We tried to improve the charging performance of flux pump. Impact of rotating speed of the flux pump on charging both the INS and NI coils will be analyzed in depth.

## II. EXPERIMENTAL SYSTEM

### A. Specifications of Insulated and Non-Insulated HTS Coil

Two double-pancake (DP) test coils were wound with YBCO coated conductor: one wound with Kapton tape (INS) and the other wound without turn-to-turn insulation (NI). The NI coil was impregnated by liquid solder at around 185 °C. [33]. Solder impregnation can prevent further oxidization of turn-to-turn contact, help fix turn-to-turn contact resistance, but significantly reduced the characteristic resistance ( $R_c$ ) [33], [35]. The INS coil was wound with the tape manufactured by *Shanghai Superconductor Technology Company (SSTC)*; the NI coil was wound with YBCO tape from *SuperPower*.

Manuscript received October 26, 2018; accepted February 7, 2019. Date of publication March 8, 2019; date of current version March 27, 2019. This work was supported by Cambridge Commonwealth, European & International Trust. (Corresponding author: Jianzhao Geng.)

J. Ma, J. Geng, J. Gawith, H. Zhang, C. Li, B. Shen, Q. Dong, J. Yang, J. Chen, and T. A. Coombs are with the Department of Engineering, University of Cambridge, Cambridge CB3 0FA, U.K. (e-mail: jg717@cam.ac.uk).

Z. Li is with the Department of Engineering, University of Cambridge, Cambridge CB3 0FA, U.K., and also with the College of Electrical Engineering, Zhejiang University, Hangzhou 310027, China.

Color versions of one or more of the figures in this paper are available online at <http://ieeexplore.ieee.org>.

Digital Object Identifier 10.1109/TASC.2019.2901915

TABLE I  
SPECIFICATIONS OF INS COIL AND NI COIL

	INS Coil	NI Coil
Tape $I_c$	100 A	95 A
Coil $I_c$	62 A	35 A
Outer Diameter	85 mm	78 mm
Inner Diameter	63 mm	63 mm
Number of Turns	30SP/60DP	32SP/64DP
Inductance	123 $\mu$ H	$\approx 120 \mu$ H
$R_c$	/	1 $\mu\Omega$

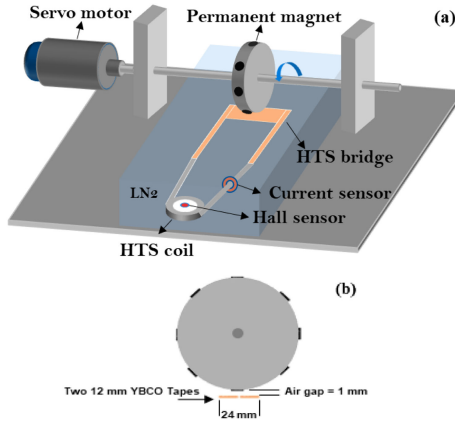


Fig. 1. (a) Schematic of experimental setup of the rotation type flux pump for HTS coils. (b) Schematic view of the rotor and HTS stator.

Table I summarizes the key parameters of INS and NI coil. Both coils have the same inner diameter (63 mm) and same number of turns (60 turns), while the outer diameter of the INS coil was 7 mm larger than NI coil, owing to the turn-to-turn Kapton insulation. The coil inductance of the INS coil is 123  $\mu$ H. The coil inductance of NI coil is not measurable by the inductance meter. We assume that the two coils have similar inductance values since they share similar geometries and same number of turns. After winding process and solder impregnation, the critical current of INS coil is 62 A and the critical current of NI coil is 35 A. The characteristic resistance ( $R_c$ ) of NI coil is quite low at around 1  $\mu\Omega$  and was calculated by the sudden open-circuit discharge curve [33].

### B. Rotating Permanent Magnets Based Flux Pump

Fig. 1 shows the schematic of the rotating permanent magnets based flux pump for the HTS coil. 8 permanent magnets are uniformly mounted on an aluminum disc with their north poles facing radially outward. The disc is mounted on a shaft, driven to rotate by a servo motor. This aluminum disc is named as a “rotor” in this study. The motor is controlled by a 0.75 kW Omron MX2 200V single phase inverter. The rotating speed can be set by the output frequency of the inverter. The permanent magnets are rare earth neodymium discs: product code MREDI 270, grading N42H. The diameter of the rare earth neodymium disc is 10 mm and the thickness is 7 mm. The diameter of the rotor is 100 mm. The motor employed in this study is Brook Hansen Type W-DA71SK motor.

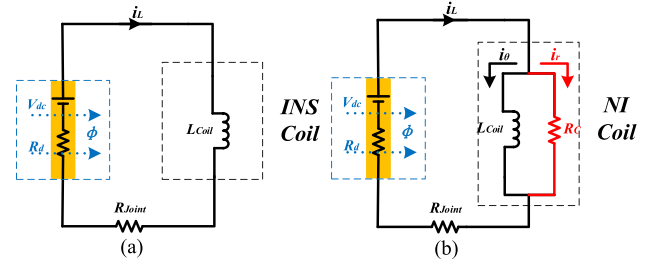


Fig. 2. Equivalent circuit of rotating permanent magnets based flux pump for (a) INS coil and (b) NI coil.

Under the rotating magnet disc, there is a HTS sheet consisted of two parallel 12-mm wide YBCO tapes. Two parallel 12-mm YBCO tapes are soldered on other two 12-mm YBCO tapes as a “stator”. The two parallel tapes are close to each other and the gap between them can be neglected. The stator is perpendicular to the magnet moving path and connected by soldering to a HTS load coil. The stator tape is manufactured by *SuNAM* and the critical current is around 600A. The air gap between the stator and the rotating disc can be adjusted. In this study, the air gap is set as 1 mm. The magnetic field density that 1 mm above the center position of neodymium magnet is around 470 mT.

During the experiment, the HTS stator and coil were placed in liquid nitrogen ( $LN_2$ ). When magnet disc rotate, a magnetic field produced by the circularly moving permanent magnets travels across the stator. This travelling magnetic field triggers a net flow from one side of stator to another side. A dc voltage ( $V_{dc}$ ) [36] and a dynamic resistance ( $R_d$ ) are generated on the stator [13], [19], [37]–[40]. The dynamic resistance is generated by an AC field perpendicular to the wide surface of the HTS stator. The stator functions as a quasi-steady DC voltage source with an inherent resistance ( $R_d$ ). The DC voltage will charge the HTS load coil, eventually to a saturated state.

The equivalent circuit of the rotating permanent magnets based flux pump for INS and NI coils is presented in Fig. 2. The  $V_{dc}$  and  $R_d$  refers to the DC voltage and dynamic resistance on the stator respectively.  $R_{joint}$  refers to the total joint resistance in the charging circuit, including joint resistance at the two ends of stator parallel tapes and the two soldering points between the coil leads and the shoulders of the stator.  $i_L$  is the load current of charging loop. In Fig. 2(b), the  $R_c$  refers to the characteristic resistance of the NI coil and the  $i_t$  is the turn-to-turn bypass current of the NI coil.  $i_\theta$  is the azimuthal current flowing through the YBCO of the NI coil.

The load current  $i_L$  was monitored by a current sensor, as shown in Fig. 1. A hall sensor was mounted at the centre of the HTS coil to monitor the magnetic field generated by the coil (denoted by  $B_{coil}$ ). For both NI and INS coil,  $i_\theta$  can be monitor by this field sensor. The voltage across the HTS coil was measured directly by a NI PCI-6221 (37-Pin) DAQ card via a pair of voltage taps.

## III. RESULTS AND ANALYSIS

### A. Charging Curve Comparison Between INS and NI Coil

In this section, the charging characteristics of INS and NI coil at different rotating speed are presented in Fig. 3(a) and (b)

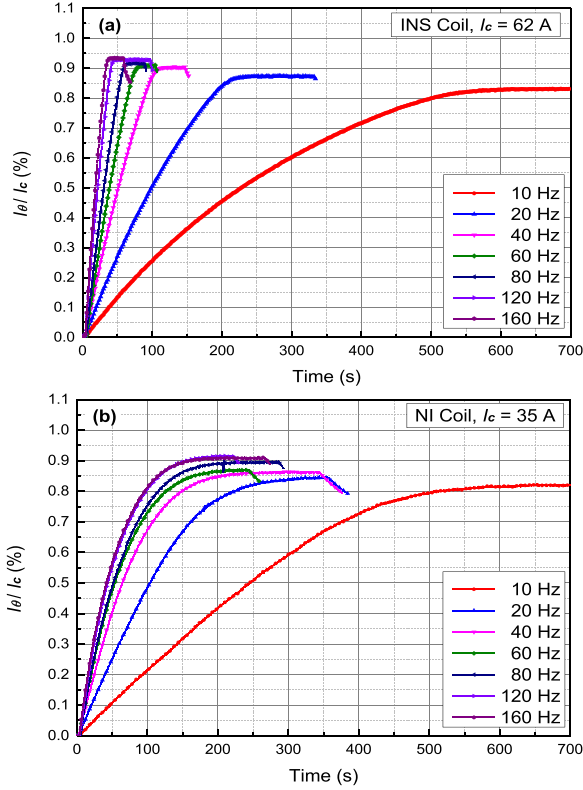


Fig. 3. Charging characteristics of (a) INS coil and (b) NI coil under different travelling wave frequency, or at different rotating speed.

respectively. The air gap between the rotor and stator is set as 1 mm. The frequency in Fig. 3 refers to frequency of the travelling wave crossing the stator which equals the number of magnets passing by the stator per second.

As shown in Fig. 3, INS coil and NI coil show different charging characteristics. The charging speed of NI coil is much slower than INS coil via the rotating permanent magnets based flux pump. When the wave frequency is 160 Hz, the charging time for NI coil is around 150 s, while it only takes around 30 s to charge the INS coil. The charging time for NI coil is 5 times of the charging time for INS coil. When the wave frequency is 40 Hz, the charging time for NI coil is around 200 s while it takes around 100 s for INS coil. But when the frequency is only 10 Hz, the charging time are almost the same for NI and INS coils. The difference in charging speeds of two coils increases when travelling wave frequency is increasing. The reason for this feature will be explained in the following Section C.

The charging curves of INS and NI coil are in different shapes. For the INS coil, there is a clear and sharp “knee” marking the transition to the current-limited “saturation zone”, which is caused by the resistance of the INS coil as the current approaches  $I_c$  of the coil. For the NI coil, the charging curve is different because a large proportion of charging current flows through the radial turn-to-turn bypass path.

### B. Frequency Dependence

The saturated coil current and the charging time of INS and NI coil with different travelling wave frequency are plotted in Fig. 4. As shown in Fig. 4(a), the saturated coil currents of both

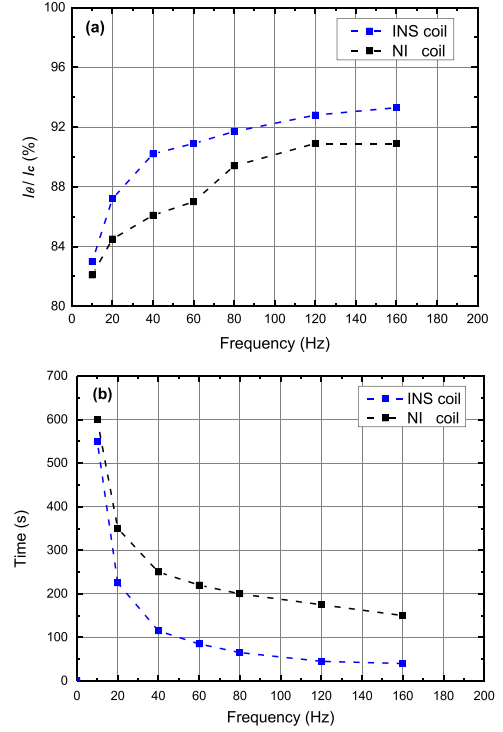


Fig. 4. (a) Saturated coil current and (b) charging time of INS and NI coil with different travelling wave frequency.

INS and NI coil increased with the increase of wave frequency. But the saturated coil current of NI coil is slightly smaller than that of INS coil at the same wave frequency. When travelling wave frequency increased from 10 Hz to 160 Hz, saturated INS coil current rose from 83% to 93.3%, while the saturated NI coil current rose from 82.1% to 90.9%. As shown in Fig. 4 (b), the charging time of both INS and NI coil decreased with the increase of wave frequency. The charging time of NI coil is much smaller than the INS coil at the same wave frequency. When travelling wave frequency increased from 10 Hz to 160 Hz, the charging time of INS coil decreased from 550 s to 40 s, while the charging time of NI coil decreased from 600 s to 150 s. Fig. 3 and Fig. 4 show that we can improve the charging performance of rotating permanent magnets based flux pump for both INS and NI coil through increasing the travelling wave frequency or magnets rotating speed.

### C. $V_{dc}$ and $R_d$ of the Stator

Here, we assume that the output dc voltage ( $V_{dc}$ ) and inherent dynamic resistance ( $R_d$ ) of rotating permanent magnets based flux pump is almost the same for both INS and NI load coils, when working at the same wave frequency with the same air gap. Based on this assumption, the  $V_{dc}$  and  $R_d$  are calculated through the charging curves of INS coil by using the following method.

Fig. 5 is an example fitting curve to calculate the  $V_{dc}$  and  $R_d$ . The data are obtained with a rate of 1 sample point per 2.5 seconds. The data are smaller than 90% saturation current, which means that the INS coil is still in superconducting state and no flux-flow resistance is generated. In this case, the

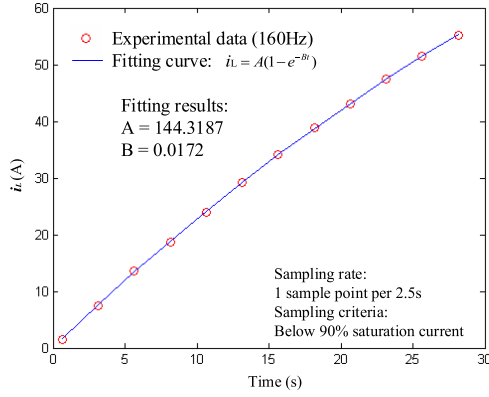


Fig. 5. An example fitting curve with experimental data from coil current of INS coil when the wave frequency is 160 Hz.

equivalent circuit of rotating permanent magnets based flux pump for INS coil is exactly the same with the circuit in Fig. 2(a), which can be expressed as:

$$L_{coil} \frac{di_L}{dt} + i_L(R_{joint} + R_d) = V_{dc} \quad (1)$$

Solving the equation (1), we can obtain:

$$i_L = A(1 - e^{-Bt}) \quad (2)$$

$$A = \frac{V_{dc}}{R_d + R_{joint}} \quad (3)$$

$$B = \frac{R_d + R_{joint}}{L_{coil}} \quad (4)$$

As shown in Fig. 5, we can get the values of parameter A and B by fitting the experimental data into equation (2) with the help of Matlab. Then  $V_{dc}$  and  $R_d$  at 120 Hz wave frequency can be calculated through solving equation (3) and (4) if  $R_{joint}$  and  $L_{coil}$  is already known.  $L_{coil} = 123 \mu\text{H}$  is already known in Table I.  $R_{joint}$  can be calculated from the equation (5):

$$R_{joint} = \frac{L_{coil}}{\tau} \quad (5)$$

where  $\tau$  is the time constant of the current decay curve of INS coil after flux pump stopped working. From the experiment result, we obtained  $\tau = 598.4 \text{ s}$ . Then,  $R_{joint} = 205.5 \text{ n}\Omega$  is calculated. Since we have the value of A, B,  $R_{joint}$  and  $L_{coil}$ ,  $V_{dc}$  and  $R_d$  can be calculated by solving equation (3) and (4). By using this method, we can calculate the  $V_{dc}$  and  $R_d$  under different frequency.

The calculated results are plotted in Fig. 6(a) and (b). The red lines are fitting functions, showing the relationship between  $V_{dc}$  (or  $R_d$ ) and travelling wave frequency. Calculated results show that both  $V_{dc}$  and  $R_d$  increase linearly with the increase of travelling wave frequency, which agree well with ref. [13]. When wave frequency increases from 10 Hz to 160 Hz,  $V_{dc}$  increases from 25  $\mu\text{V}$  to 300  $\mu\text{V}$  and  $R_d$  increases from 150  $\text{n}\Omega$  to 1900  $\text{n}\Omega$ . Both  $V_{dc}$  and  $R_d$  can be expressed as a linear function of wave frequency, and the stator functions as a DC voltage source ( $V_{dc}$ ) with an inherent resistance ( $R_d$ ).

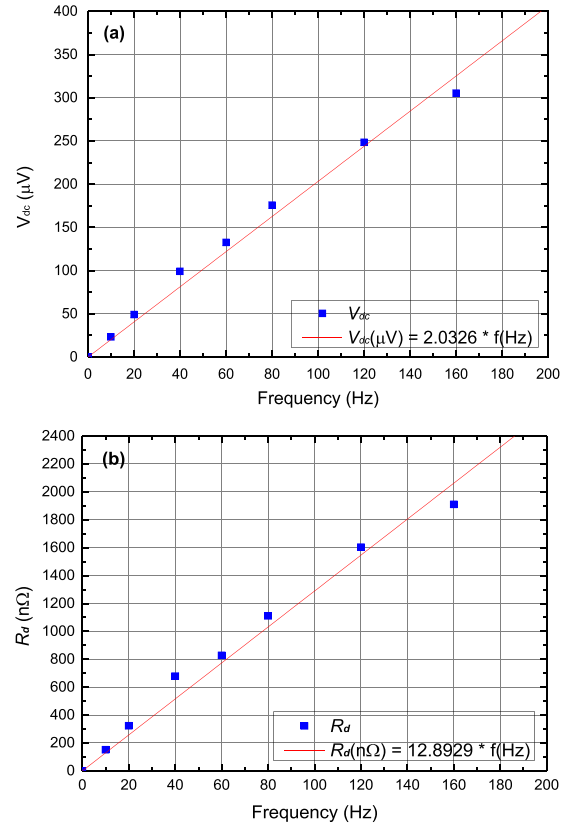


Fig. 6. (a) Calculated  $V_{dc}$  and (b)  $R_d$  from equation (3) and equation (4).

According to Fig. 2(b), the ramping equations for NI coil are:

$$V_{dc} - i_L(R_{joint} + R_d) = L_{coil} \frac{di_L}{dt} = i_r R_c \quad (6)$$

$$i_L = i_r + i_\theta \quad (7)$$

Solving the above equation (6) and (7), we obtain:

$$i_L = C(1 - e^{-Dt}) \quad (8)$$

$$C = \frac{V_{dc}}{R_d + R_{joint}} \quad (9)$$

$$D = \frac{R_c(R_d + R_{joint})}{L_{coil} \cdot (R_c + R_d + R_{joint})} \quad (10)$$

The characteristic charging time for the NI and INS coil are:

$$\tau_{NI} = \frac{1}{D} = \frac{L_{coil} \cdot (R_c + R_d + R_{joint})}{R_c(R_d + R_{joint})} \quad (11)$$

$$\tau_{INS} = \frac{1}{B} = \frac{L_{coil}}{(R_d + R_{joint})} \quad (12)$$

We can see that:

$$\tau_{NI} = \frac{(R_c + R_d + R_{joint})}{R_c} \cdot \tau_{INS} \quad (13)$$

We already know  $R_c = 1 \mu\Omega$  as shown in Table I. In Fig. 2(b),  $R_{joint} = 176.5 \text{ n}\Omega$  is also calculated from the current decay curve of NI coil after flux pump stopped working, which is in about the same level of joint resistance (205.5  $\text{n}\Omega$ ) in INS coil charging circuit as shown in Fig. 2(a).



Equation (13) reveals that the characteristic charging time of the NI coil will be longer (by a factor of  $(R_c + R_{\text{joint}} + R_d)/R_c$ ) than that of INS coil. This factor depends mainly on the relative magnitude of  $R_d$  and  $R_c$ . It increases significantly when working frequency rises from 10 Hz to 160 Hz, because  $R_d$  increases from 150 n $\Omega$  (much smaller level than  $R_c = 1 \mu\Omega$ ) to 1900 n $\Omega$  (relatively larger than  $R_c = 1 \mu\Omega$ ). In low working frequency,  $R_c \gg (R_{\text{joint}} + R_d)$ ,  $\tau_{\text{NI}}$  is similar in magnitude with (or slightly larger than)  $\tau_{\text{INS}}$ . But in high working frequency,  $R_c \ll (R_{\text{joint}} + R_d)$ , so  $\tau_{\text{NI}} \gg \tau_{\text{INS}}$ . This means: at higher working frequencies, the NI coil takes substantially longer time to reach saturation, which is consistent with the comparison between Fig. 3 and Fig. 4(b).

#### IV. CONCLUSION

In this paper, we compared the charging performance of an HTS rotating permanent magnets based flux pump for two different types of HTS coils: an INS coil and a NI coil. The experimental results show that the flux pump works well for both two types of HTS coils. However, compared with INS coil, the charging speed of NI coil is much slower, especially at higher operating frequency. This phenomenon is analyzed in details in this paper. Experimental results also show that increasing the magnets rotating speed can improve the charging performance for both INS and NI coil. We found out that the DC voltage ( $V_{\text{dc}}$ ) and inherent dynamic resistance ( $R_d$ ) generated on the HTS stator section increases linearly with the increase of rotating speed.

#### ACKNOWLEDGMENT

The authors would like to thank the Cambridge Trust, Engineering Department and Churchill College of Cambridge University, and Ford of Britain Fund for the conference grant. J Ma would also like to acknowledge Cambridge Trust and CSC for the scholarship to support his study in Cambridge.

#### REFERENCES

- [1] Y. Iwasa et al., "A high-resolution 1.3-GHz/54-mm LTS/HTS NMR magnet," *IEEE Trans. Appl. Supercond.*, vol. 25, no. 3, Jun. 2015, Art. no. 4301205.
- [2] G. Ma et al., "Experiment and simulation of REBCO conductor coils for an HTS linear synchronous motor," *IEEE Trans. Appl. Supercond.*, vol. 27, no. 4, Jun. 2017, Art. no. 5201805.
- [3] G. Ma, H. Liu, X. Li, H. Zhang, and Y. Xu, "Numerical simulations of the mutual effect among the superconducting constituents in a levitation system with translational symmetry," *J. Appl. Phys.*, vol. 115, no. 8, Feb. 2014, Art. no. 083908.
- [4] W. D. Markiewicz et al., "Design of a superconducting 32 T magnet with REBCO high field coils," *IEEE Trans. Appl. Supercond.*, vol. 22, no. 3, Jun. 2012, Art. no. 4300704.
- [5] Y. Yoon, J. Kim, H. Lee, S. Hahn, and S. Moon, "26 T 35 mm all-GdBa2Cu3O7-x multi-width no-insulation superconducting magnet," *Supercond. Sci. Technol.*, vol. 29, no. 4, Apr. 2016, Art. no. 04LT04.
- [6] S. Hahn, D. K. Park, J. Bascunan, and Y. Iwasa, "HTS pancake coils without turn-to-turn insulation," *IEEE Trans. Appl. Supercond.*, vol. 21, no. 3, pp. 1592–1595, Jun. 2011.
- [7] S. Hahn, D. K. Park, J. Voccio, J. Bascunan, and Y. Iwasa, "No-insulation (NI) HTS inserts for > 1 GHz LTS/HTS NMR magnets," *IEEE Trans. Appl. Supercond.*, vol. 22, no. 3, Jun. 2012, Art. no. 4302405.
- [8] S. Choi, H. C. Jo, Y. J. Hwang, S. Hahn, and T. K. Ko, "A study on the no insulation winding method of the HTS coil," *IEEE Trans. Appl. Supercond.*, vol. 22, no. 3, Jun. 2012, Art. no. 4904004.
- [9] Y. G. Kim, S. Hahn, K. L. Kim, O. J. Kwon, and H. Lee, "Investigation of HTS racetrack coil without turn-to-turn insulation for superconducting rotating machines," *IEEE Trans. Appl. Supercond.*, vol. 22, no. 3, Jun. 2012, Art. no. 5200604.
- [10] K. Kim et al., "Design and performance estimation of a 35 T 40 mm no-insulation all-REBCO user magnet," *Supercond. Sci. Technol.*, vol. 30, no. 6, Jun. 2017, Art. no. 065008.
- [11] X. Wang et al., "Turn-to-turn contact characteristics for an equivalent circuit model of no-insulation REBCO pancake coil," *Supercond. Sci. Technol.*, vol. 26, no. 3, Jan. 2013, Art. no. 035012.
- [12] C. Hoffmann, D. Pooke, and A. D. Caplin, "Flux pump for HTS magnets," *IEEE Trans. Appl. Supercond.*, vol. 21, no. 3, pp. 1628–1631, Jun. 2011.
- [13] Z. Jiang, K. Hamilton, N. Amemiya, R. A. Badcock, and C. W. Bumby, "Dynamic resistance of a high-Tc superconducting flux pump," *Appl. Phys. Lett.*, vol. 105, no. 11, Sep. 2014, Art. no. 112601.
- [14] S. Lee et al., "Persistent current mode operation of a 2G HTS coil with a flux pump," *IEEE Trans. Appl. Supercond.*, vol. 26, no. 4, Jun. 2016, Art. no. 0606104.
- [15] C. W. Bumby et al., "Development of a brushless HTS exciter for a 10 kW HTS synchronous generator," *Supercond. Sci. Technol.*, vol. 29, no. 2, Jan. 2016, Art. no. 024008.
- [16] K. Hamilton, A. E. Pantoja, J. G. Storey, Z. Jiang, R. A. Badcock, and C. W. Bumby, "Design and performance of a "Squirrel-Cage" dynamo-type HTS flux pump," *IEEE Trans. Appl. Supercond.*, vol. 28, no. 4, Jun. 2018, Art. no. 5205705.
- [17] Z. Bai, G. Yan, C. Wu, S. Ding, and C. Chen, "A novel high temperature superconducting magnetic flux pump for MRI magnets," *Cryogenics*, vol. 50, no. 10, pp. 688–692, Oct. 2010.
- [18] L. Fu, K. Matsuda, T. Lecrevisse, Y. Iwasa, and T. A. Coombs, "A flux pumping method applied to the magnetization of YBCO superconducting coils: frequency, amplitude and waveform characteristics," *Supercond. Sci. Technol.*, vol. 29, no. 4, Apr. 2016, Art. no. 04LT01.
- [19] J. Geng and T. A. Coombs, "Mechanism of a high-Tc superconducting flux pump: Using alternating magnetic field to trigger flux flow," *Appl. Phys. Lett.*, vol. 107, no. 14, Oct. 2015, Art. no. 142601.
- [20] J. Geng, K. Matsuda, L. Fu, B. Shen, X. Zhang, and T. A. Coombs, "Operational research on a high-Tc rectifier-type superconducting flux pump," *Supercond. Sci. Technol.*, vol. 29, no. 3, Feb. 2016, Art. no. 035015.
- [21] C. W. Bumby et al., "Anomalous open-circuit voltage from a high-Tc superconducting dynamo," *Appl. Phys. Lett.*, vol. 108, no. 12, Mar. 2016, Art. no. 122601.
- [22] C. W. Bumby et al., "Frequency dependent behavior of a dynamo-type HTS flux pump," *IEEE Trans. Appl. Supercond.*, vol. 27, no. 4, Jun. 2017, Art. no. 5200705.
- [23] A. E. Pantoja, J. G. Storey, R. A. Badcock, Z. Jiang, S. Phang, and C. W. Bumby, "Output during continuous frequency ramping of a dynamo-type HTS flux pump," *IEEE Trans. Appl. Supercond.*, vol. 28, no. 3, Apr. 2018, Art. no. 5202205.
- [24] Z. Jiang, C. W. Bumby, R. A. Badcock, H. Sung, N. J. Long, and N. Amemiya, "Impact of flux gap upon dynamic resistance of a rotating HTS flux pump," *Supercond. Sci. Technol.*, vol. 28, no. 11, Sep. 2015, Art. no. 115008.
- [25] A. E. Pantoja, Z. Jiang, R. A. Badcock, and C. W. Bumby, "Impact of stator wire width on output of a dynamo-type HTS flux pump," *IEEE Trans. Appl. Supercond.*, vol. 26, no. 8, Dec. 2016, Art. no. 4805208.
- [26] R. A. Badcock et al., "Impact of magnet geometry on output of a dynamo-type HTS flux pump," *IEEE Trans. Appl. Supercond.*, vol. 27, no. 4, Jun. 2017, Art. no. 5200905.
- [27] J. G. Storey, A. E. Pantoja, Z. Jiang, K. Hamilton, R. A. Badcock, and C. W. Bumby, "Impact of annular yoke geometry on performance of a dynamo-type HTS flux pump," *IEEE Trans. Appl. Supercond.*, vol. 28, no. 3, Apr. 2018, Art. no. 5203906.
- [28] H. J. Sung, R. A. Badcock, Z. Jiang, J. Choi, M. Park, and I. K. Yu, "Design and heat load analysis of a 12 MW HTS wind power generator module employing a brushless HTS exciter," *IEEE Trans. Appl. Supercond.*, vol. 26, no. 4, Jun. 2016, Art. no. 5205404.
- [29] H. Jeon et al., "Methods for increasing the saturation current and charging speed of a rotary HTS flux-pump to charge the field coil of a synchronous motor," *IEEE Trans. Appl. Supercond.*, vol. 28, no. 3, Apr. 2018, Art. no. 5202605.

- [30] H. Jeon *et al.*, "PID control of an electromagnet-based rotary HTS flux pump for maintaining constant field in HTS synchronous motors," *IEEE Trans. Appl. Supercond.*, vol. 28, no. 4, Jun. 2018, Art. no. 5207605.
- [31] H. Zhang *et al.*, "Magnetization of coated conductor stacks using flux pumping," *IEEE Trans. Appl. Supercond.*, vol. 27, no. 4, Jun. 2017, Art. no. 8200205.
- [32] Y. H. Choi, S. Kim, S. Jeong, J. H. Kim, H. M. Kim, and H. Lee, "A study on charge-discharge characteristics of no-insulation GdBCO magnets energized via a flux injector," *IEEE Trans. Appl. Supercond.*, vol. 27, no. 4, Jun. 2017, Art. no. 4601206.
- [33] J. Ma, J. Geng, and T. A. Coombs, "Flux pumping for non-insulated and metal-insulated HTS coils," *Supercond. Sci. Technol.*, vol. 31, no. 1, Dec. 2017, Art. no. 015018.
- [34] J. Ma, J. Geng, J. Gawith, and T. A. Coombs, "High-Temperature Superconducting (HTS) Transformer-rectifier flux pump for powering no-insulation superconducting magnets with low characteristic resistance," *Phys. C: Supercond. Appl.*, vol. 560, pp. 1–6, Feb. 2019.
- [35] Y. Li *et al.*, "Feasibility study of the impregnation of a no-insulation HTS coil using solder," *IEEE Trans. Appl. Supercond.*, vol. 28, no. 1, Jan. 2018, Art. no. 5200505.
- [36] J. Geng *et al.*, "Origin of dc voltage in type II superconducting flux pumps: field, field rate of change, and current density dependence of resistivity," *J. Phys. D: Appl. Phys.*, vol. 49, no. 11, Mar. 2016, Art. no. 11LT01.
- [37] V. V. Andrianov, V. B. Zenkevich, V. V. Kurguzov, V. V. Sychev, and F. F. Ternovskii, "Effective resistance of an imperfect type-II superconductor in an oscillating magnetic field," *Sov. J. Exp. Theor. Phys.* vol. 31, pp. 815–819, 1970.
- [38] T. Ogasawara, K. Yasuköchi, S. Nose, and H. Sekizawa, "Effective resistance of current-carrying superconducting wire in oscillating magnetic fields 1: Single core composite conductor," *Cryogenics*, vol. 16, no. 1, pp. 33–38, Jan. 1976.
- [39] M. P. Oomen, J. Rieger, M. Leghissa, B. ten Haken, and H. H. J. ten Kate, "Dynamic resistance in a slab-like superconductor with  $J_c(B)$  dependence," *Supercond. Sci. Technol.*, vol. 12, no. 6, pp. 382–387, 1999.
- [40] A. Uksusman, Y. Wolfus, A. Friedman, A. Shaulov, and Y. Yeshurun, "Voltage response of current carrying Y–Ba–Cu–O tapes to alternating magnetic fields," *J. Appl. Phys.*, vol. 105, no. 9, Jun. 2009, Art. no. 093921.